JGR Atmospheres

RESEARCH ARTICLE
10.1029/2021JD035821

Key Points:

- Unusual plasma formations (UPFs) can occur inside the initial corona streamer burst, before the development (or in the absence) of hot leader channel
- UPFs contain hot channel segments that are formed, possibly via the thermal-ionizational instability, on a time scale of 1 μs or less
- UPFs occurred in the vicinity of cloud boundary, where the electric field is highest, as this boundary is penetrated by the streamer burst

Correspondence to:
A. Yu. Kostinskiy,
kostinsky@gmail.com

Citation:
Kostinskiy, A. Yu., Bogatov, N. A., Syssoev, V. S., Mareev, E. A., Andreev, M. G., Bulatov, M. U., et al. (2022). Unusual plasma formations produced by positive streamers entering the cloud of negatively charged water droplets. *Journal of Geophysical Research: Atmospheres*, *127*, e2021JD035821. https://doi.org/10.1029/2021JD035821

Received 7 SEP 2021
Accepted 7 OCT 2022

Unusual Plasma Formations Produced by Positive Streamers Entering the Cloud of Negatively Charged Water Droplets

A. Yu. Kostinskiy[1], N. A. Bogatov[2], V. S. Syssoev[3], E. A. Mareev[2], M. G. Andreev[1], M. U. Bulatov[3], D. I. Sukharevsky[3], and V. A. Rakov[4]

[1]National Research University Higher School of Economics, Moscow, Russia, [2]Institute of Applied Physics RAS, Nizhny Novgorod, Russia, [3]High-Voltage Research Center of the All-Russian Scientific Research Institute of Technical Physics, Istra, Russia, [4]Department of Electrical and Computer Engineering, University of Florida, Gainesville, FL, USA

Abstract Kostinskiy et al. (2015b), https://doi.org/10.1002/2015GL065620, using a high-speed infrared (2.5–5.5 μm) camera, discovered the so-called unusual plasma formations (UPFs) in artificial clouds of charged water droplets. UPFs had complex morphology including both streamer-like regions and hot channel segments. They were observed both in the presence and in the absence of hot leader channels developing from the grounded plane toward the cloud. In this paper, which is aimed at revealing the genesis of UPFs, we present two UPFs that occurred inside the initial corona streamer burst of positive polarity emitted from the grounded plane, prior to the formation (or in the absence) of associated hot leader channel. These streamer bursts developed at speeds of 5–7 × 10^5 m/s over 1–1.5 m before entering the optically visible negatively charged cloud and producing UPFs at its periphery. Hot channel segments within UPFs were formed in very short times of the order of 1 μs or less. It is not clear if the UPFs were caused solely by the enhanced electric field near the charged cloud boundary or other factors also played a role. Occurrence of UPFs may be a necessary component of the lightning initiation process.

1. Introduction

Kostinskiy et al. (2015a, 2015b), using a framing camera operating in the infrared (IR) range of 2.5–5.5 μm, have discovered a new class of electric discharges within artificial clouds of charged water droplets with typical radii of 0.3–0.5 μm (considerably smaller than the IR wavelengths) and termed those discharges unusual plasma formations (UPFs). In the IR images, some UPF segments had similar or even greater brightness than the positive upward leader channel imaged in the same frame, suggesting that the temperature of those UPF segments is comparable to that of upward positive leaders. The upward positive leaders were preceded by initial positive corona streamer bursts, both originating from a small sphere on the grounded plane and propagating over 1 m or so toward the negatively charged cloud. Hundreds of IR images of UPFs were obtained and examined, with many examples being presented by Kostinskiy et al. (2015a, 2015b), but only a few UPFs were recorded in the visible range. This is the case because UPFs occur primarily inside the cloud where visible light (whose wavelengths are comparable to the water droplet size) experiences strong scattering.

The goal of this work was to examine the genesis of UPFs; that is, to gain new insights into the dynamics of UPFs and draw some inferences about the mechanism of their initiation and development. This was impossible with the IR records, for which the exposure time was as large as 2–3 ms. We supplemented the experimental setup used by Kostinskiy et al. (2015a, 2015b) by microwave diagnostics (Bogatov et al., 2020) and acquired additional data, including good visible-range images of two UPFs which occurred outside (near the edge of) the cloud. In contrast to the IR camera, the visible-range camera operated with microsecond-scale exposure times, which was sufficient for resolving the UPF occurrence context. We also recorded the electric current at the grounded sphere and the time of luminosity onset in the cloud (with a photomultiplier tube). Our overall data set is unique, and the results constitute the first experimental evidence of a scenario in which UPFs can occur.

In this article, we use the term "long streamers" in referring to streamers that have essentially lost their galvanic (electrical) connection with their origin. Streamer is a cold plasma formation composed of a brighter head and a much fainter tail. Part of the tail, which is closer to the head, contains a significant number of free electrons and therefore is conducting. The characteristic length of the conducting part of streamer tail can be roughly estimated based on the speed of movement of streamer head v_{str} and the characteristic electron loss time scale τ_a due to attachment and recombination, which is of the order of tens of nanoseconds (e.g., Francisco et al., 2021, Figure

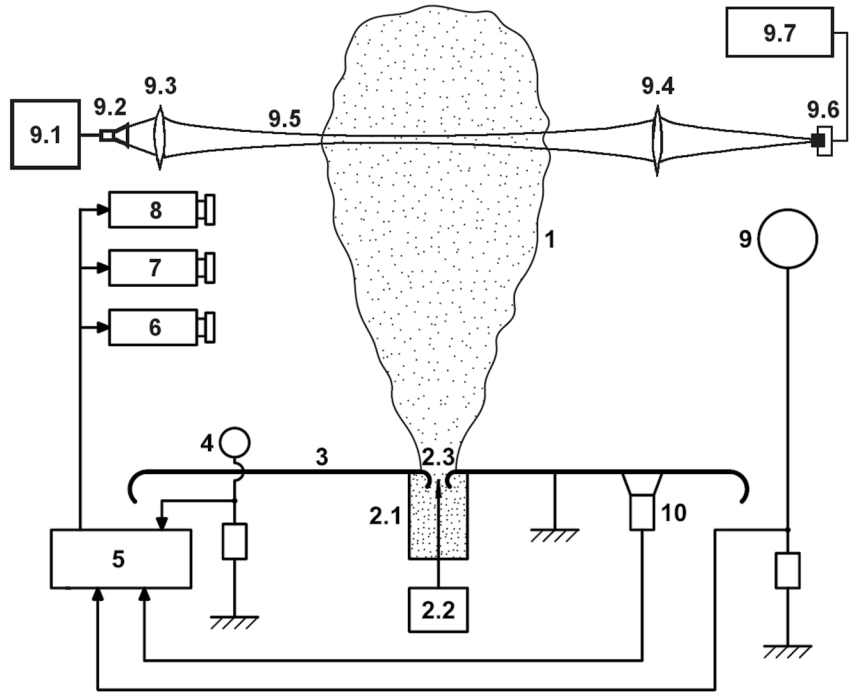

Figure 1. Experimental setup: 1: cloud of negatively charged water droplets, 2.1: steam generator, 2.2: high-voltage source with corona-producing sharp point, 2.3: nozzle, 3: grounded metal plane, 4: 5-cm sphere connected to ground via current-measuring shunt, 5: oscilloscope, 6: visible-range high-speed framing camera 4Picos, 7: infrared high-speed framing camera FLIR-7700, 8: photomultiplier, 9.1: microwave generator G4-91, 9.2: horn antenna, 9.3 and 9.4: dielectric lenses, 9.5: microwave beam, 9.6: receiving waveguide, microwave amplifier, and a microwave diode, 9.7: oscilloscope, 10: 50-cm sphere for monitoring variations of cloud charge, and 11: pulse generator.

4; Kossyi et al., 1992; Li et al., 2022, Figure 8). We assume that $\tau_a \approx 50$ ns ($5 \cdot 10^{-8}$ s) and that the characteristic time scale for the corresponding loss of conductivity $\tau_c \approx 15\tau_a = 7.5 \cdot 10^{-7}$s. During this time, the conductivity would decrease by a factor of $e^{15} \approx 3 \cdot 10^6$ (e.g., from 10^{-5} S/m to $3 \cdot 10^{-12}$ S/m). The range of speeds for positive streamers is approximately $(2-8) \cdot 10^7$cm/s (e.g., Bazelyan & Raizer, 1998), so that the length of the conducting part of streamer tail $L_{str} \approx v_{str} \cdot \tau_c = 15 - 60$ cm. Thus, streamers whose heads moved farther than 15–60 cm from their origin are considered here as long streamers. A recent review of streamer discharges is found in Nijdam et al. (2020).

It is worth noting that, as of today, UPFs have been observed only inside or near the artificial jet-shaped clouds of small (fraction of a micrometer) water droplets.

1.1. Experimental Setup

The experiments were performed at the High-Voltage Research Center of the Zababakhin All-Russian Scientific Research Institute of Technical Physics, Istra (http://www.ckp-rf.ru/usu/73578/). The experimental setup used in this study (Figure 1) was similar to the one used in previous studies and described in detail by Kostinskiy et al. (2015a, 2015b, 2016). Charged cloud (1) was created by steam generator (2.1) and high-voltage source (2.2) coupled with the corona-producing sharp point (needle). The latter was located in the nozzle (2.3) which the steam-air jet was passing through. The steam in the nozzle had a temperature of about 100–120°C and a pressure in the range of 0.2–0.6 MPa. The steam moved at an initial speed of about 400–420 m/s with an aperture angle of 28°, forming a submerged turbulent jet. The nozzle with the needle was located in the center of a grounded plane (3) with a diameter of 2 m. As a result of rapid cooling, the vapor condensed into water droplets with an average radius of about 0.3–0.5 μm. Ions produced by corona discharge between the tip of the needle and the nozzle (2.3) served to charge the water droplets. The corona-producing needle was energized by a 10–20 kV DC voltage source. The current carried by the charged aerosol jet was in the range from 60 to 150 μA. The steam-air jet is

rapidly decelerated in the ambient air and creates a highly turbulent motion of a two-phase charged flow. As a result, the jet-shaped cloud does not have a smooth visible boundary anywhere. In each experiment, we could only approximately determine the boundary of the cloud in the visible range; that is, we could only determine the part of the cloud, through which we could not see objects located behind the cloud. But this does not mean that there are no charged droplets at other points in the space between the cloud and the grounded plane, since their density could be low enough to allow us to see through that part of the cloud. The visible structure of the cloud depends on the relative humidity, temperature, and wind direction, since the evaporation of droplets and their movement depend on these parameters. The approximate jet-shaped cloud boundary is shown in the IR image in Figure 4 (left panel) along with the UPF occurring at that boundary. We think that the strong cloud turbulence can influence the initiation of UPFs, but, as of today, there is no evidence of that.

When the total charge accumulated in the cloud reached ~60 μC, meter-scale sparks spontaneously appeared between the nearby grounded objects and the cloud. In the case of negatively charged cloud, the sparks usually occurred as a sequence of an initial positive corona streamer burst and a positive leader, both developing from the grounded metal sphere (4) toward the cloud (1). The metal sphere had a diameter of 5 cm and was located at a distance of 0.85 m from the center of the grounded plane (3). The top point of the sphere was 12 cm above the plane. Initial positive corona streamer bursts and positive leaders, originating from the metal sphere, propagated essentially perpendicular to the direction of the diagnostic microwave beam (9.5).

Currents of initial corona streamer bursts and upward positive leaders were measured by a low-inductance 1-Ω shunt, inserted between the metal sphere (4) and ground, and a digitizing oscilloscope (5). Once the current exceeds a preset threshold value, the oscilloscope (5) records (a) the current through the shunt, (b) the discharge luminosity signal from the photomultiplier tube (PMT) (8), and (c) the signal from the 50-cm diameter metal sphere (10), used for monitoring the variation of cloud charge. The oscilloscope also outputs a trigger signal for the pulse generator (11) which forms a TTL pulse triggering high-speed cameras 4Picos (6) and FLIR SC7700M (7), as well as a second oscilloscope (9.7) recording microwave radiation (9.5) that passed through the cloud (1). The IR framing camera FLIR SC7700M ($\lambda \approx 2.5$–5.5 μm) operated at 412 frames per second (exposure time was 2.4 ms), with the image size on the matrix being 320 × 256 pixels. The IR-camera was equipped with a germanium lens with a focal length of 50 mm and an aperture of *f*/2. The 4Picos high-speed visible-range (actually it includes a portion of the UV range; $\lambda = 315$–850 nm) camera with image amplification (optical gain was 10^4) captured images on a 1,360 × 1,024-pixel matrix with exposure time from 50 ns to 10 μs. It can produce only two frames with selectable interframe interval of 500 ns or more. The 4Picos camera was equipped with a glass lens with a focal length of 50 mm and an aperture of *f*/0.95. The cameras were installed at a distance of 6.5 m from the nozzle, which forms the aerosol cloud (2.3) in the direction of the propagation axis of the microwave beam. The viewing angle (directional diagram) of the photomultiplier was ~10°, and the size of the photomultiplier's field of view at the location of the cloud was ~1 m^2. The photomultiplier tube was aimed at the upper half of the cloud, at a height of about 0.8–1 m above the plane. The time constant of the PMT was several milliseconds, but still it could fairly accurately record the onset of luminosity in its field of view.

The source of microwave radiation was a G4-91 generator (9.1). The generator output power was 5 mW, and the radiation frequency was 35 GHz ($\lambda = 8.5$ mm). The generator was operating in continuous mode. A converging microwave beam with a Gaussian profile was formed by a horn antenna (9.2) and dielectric lenses (9.3 and 9.4). The waist of the microwave beam (9.5) was located on the axis of the cloud. The angle between the axis of the microwave beam and the axis of the cloud was 85°–87°. The diameter of the microwave beam in the waist region was ~10 cm (in the studied region, the beam was almost cylindrical, and in the region of the visible edge of the aerosol cloud it was only 3% wider than at its center). The distance from the axis of the microwave beam to the grounded plane was ~1 m. The polarization of microwave radiation was linear (vertical). Microwave radiation transmitted through the cloud was focused by a dielectric lens (9.4) into the open end of the receiving waveguide, amplified with a 20 dB microwave amplifier, and detected with a microwave diode (9.6). The output level of the signal from the microwave diode was recorded with an oscilloscope (9.7). The relative attenuation of microwave radiation passing through the cloud was determined by the ratio of the value of the output signal level from the diode to the unperturbed level (in the absence of the cloud). The main source of noise that determines the sensitivity of microwave diagnostics in general was the instability of the output power of the microwave generator, which was ~10^{-3}; the latter value determined the minimum relative attenuation of the probing microwave radiation that we could register. Either an uncharged cloud or a charged cloud in absence of any discharge activity did not noticeably attenuate the probing microwave radiation. The equipment was installed in three electromagnetically

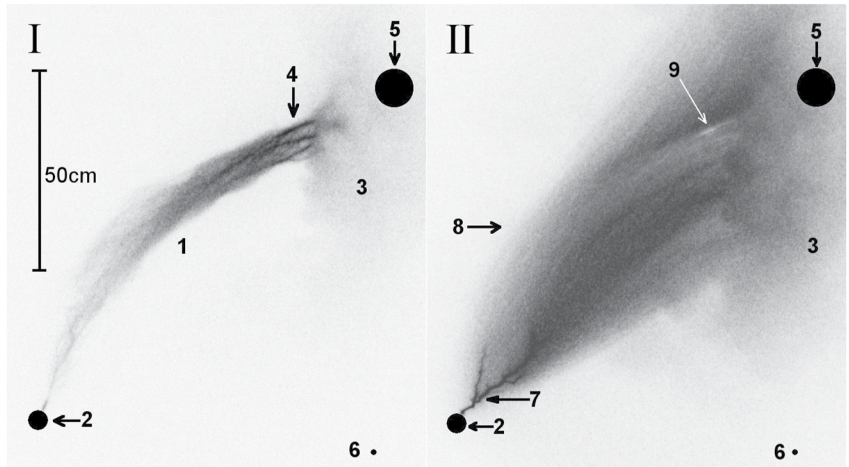

Figure 2. Two consecutive frames of event 2015-12-04_03 obtained with a visible-range 4Picos camera with image enhancement. Frames I and II had 2 and 10 μs exposure times, respectively, and the time interval between frames was 1 μs. Both frames are inverted and cropped. 1: The initial positive corona streamer burst converted to UPF; 2: 5-cm grounded sphere equipped with a current-measuring shunt; 3: cloud of negatively charged water droplets (see also 11 in Figure 4); 4: hot channel segments embedded in UPF; 5: the region of passage of the microwave beam; 6: the center of the grounded plane where the nozzle (see Figure 1) is located; 7: channel of upward positive leader; 8: streamer zone of the upward positive leader; and 9: white streak, which is an image artifact.

shielded structures/enclosures, of which two smaller ones (housing the high-speed cameras 6 and 7 and the receiving part of the microwave diagnostics setup 9.6; see Figure 1) had autonomous power supply.

1.2. Experimental Results

Presented in Figure 2 is a sequence of two 4Picos frames separated by a time interval of 1 μs. The first frame (labeled I; exposure time of 2 μs) shows the initial corona streamer burst that originated from the grounded sphere in the lower left corner and entered the negatively charged cloud in the upper right corner. Also seen in the first frame is a UPF containing three bright channel segments, which are similar to those reported by Kostinskiy et al. (2015b) and inferred by them to be hot (having gas temperature similar to that of leader channels; it is in this sense that we refer to those segments being "hot"). The second frame (labeled II; exposure time of 10 μs) shows the upward positive leader composed of a relatively short, branched hot channel and a relatively large streamer zone which enters the cloud in the upper right corner. Clearly, the UPF occurred inside the initial corona streamer burst, before the development of hot leader channel from the grounded sphere. Further, it occurred in the vicinity of the visible cloud boundary, where the electric field is expected to be highest, as that boundary was penetrated by the streamer burst. It is logical to assume that the streamer burst entering the cloud experienced some kind of instability (e.g., thermal-ionizational instability (Bychkov et al., 2007; Nighan, 1977; Raizer, 1991, pp. 222–226; Wolf et al., 2020; Zhong et al., 2019)) that led to its conversion to UPF. In the following, we will use the entirety of our experimental data (see Figures 3 and 4) to estimate the time needed for conversion of streamer burst to UPF seen in Figure 2. An additional example of such conversion is presented in Figures 5a and 5b.

The initial corona streamer burst precedes the formation of hot leader channel (this is why it is referred to as initial), although sometimes no following leader is formed. Current associated with those two processes in the first event we are going to present exhibits the initial pulse labeled 1 Figure 3b followed by a time interval with very low current level and then by a much larger in amplitude and longer in duration current waveform with multiple peaks or superimposed pulses (the overall current waveform is best seen in Figure 3a), the first three of which are labeled 2, 3, and 4 in Figure 3b. Current pulse 1 occurred before the first 4Picos frame and current peaks 2 and 3 occurred during that frame, which shows no leader channel. Therefore, we attribute current pulse 1 and current peaks 2 and 3 to the initial corona streamer burst, while current peak 4 and the following part of the large current waveform could be formed in the presence of leader channel. It is likely that the UPF was associated with current pulse 1. Note that there is a small pulse during the low-current interval, which appears to coincide with the onset of the photomultiplier signal originating from the upper part of the cloud. It is not clear if it was

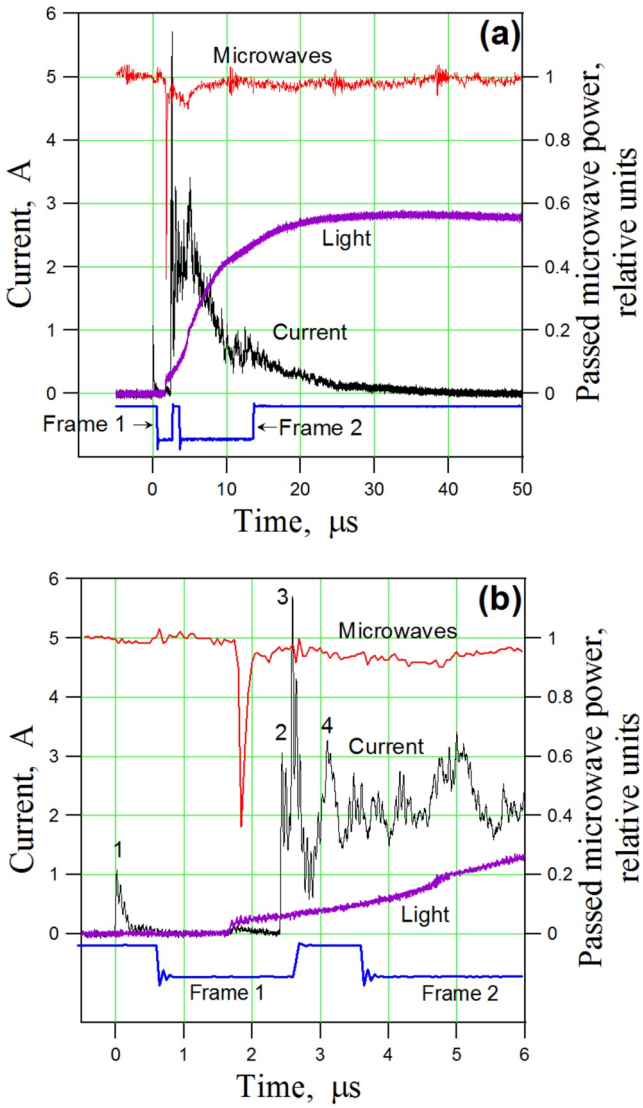

Figure 3. (Event 2015-12-04_03) (a) Current measured at the grounded sphere (shown in black); absorption of microwave radiation that passes through the cloud (shown in red and labeled "Microwaves"); photomultiplier signal (shown in purple and labeled "Light"), and exposure times of 4Picos Frames 1 and 2 (shown in blue and labeled I and II in Figure 2). Panel (b) same as panel (a), but shown on an expanded time scale. The first four major current pulses are numbered in panel (b).

just a minor variation of the low-level current or it was somehow related to the streamer burst to UPF conversion process. Interestingly, the small current pulse seems to be coincident with the beginning of appreciable cloud-charge variation (not shown here), detected with 50-cm sphere 10 (see Figure 1).

One can see in Figure 2I those streamers of the initial corona streamer burst (1), once they entered the cloud (3), were moving toward the microwave beam (5). The fact that the streamers did reach the position of microwave beam is evidenced by a pronounced microwave absorption pulse with an FWHM of about 135 ns and its peak being within the exposure time of the first 4Picos frame (left frame labeled I in Figure 2), approximately 0.85 μs before the end of exposure of that frame. It is worth noting that corona streamers in long sparks cause stronger absorption of microwave radiation than leader channels (Bogatov et al., 2020). The streamer heads traversed an arc-like trajectory between the grounded sphere (2) and the region of the microwave beam (5) in the cloud (3). The length of that trajectory was about $S_{st} \approx 1.2$ m and the streamer-head travel time was about $\tau_{st} \approx 1.7$ μs (estimated as the time interval between the peak of the current pulse 1 (see Figure 3b), associated with the onset of the initial corona streamer burst at the grounded sphere, and the onset of microwave absorption signal). Thus, the average 2D speed of streamers of the initial corona streamer burst was about $v_{st} \approx S_{st}/\tau_{st} \approx 7 \cdot 10^5$ m/s.

Also seen in Figure 2I is a UPF with three bright channel segments (4), which are partially outside of the optically opaque part of the cloud and are similar to those recorded in previous experiments by Kostinskiy et al. (2015b) and inferred by them to be relatively hot. Since the bright segments of UPFs are located at a distance of about 1 m from the origin of the initial corona streamer burst (grounded sphere), and the average velocity of streamer propagation is about 7×10^5 m/s, the process of transition of streamer burst to UPF began approximately 1.4 μs (1 m/7 $\times$ 10^5 m/s) or more after the start of the initial corona streamer burst. The time interval between the onset of the initial corona streamer burst (current pulse labeled 1 in Figure 3b) and the end of exposure of the first frame of 4Picos was 2.5 μs. Since the UPF was formed before the end of the exposure of this frame, its formation process took no more than 1.1 μs (2.5–1.4 μs).

In the second frame of 4Picos (right frame labeled II in Figure 2), the channel of upward positive leader (7) and its streamer zone (8) are clearly visible. The maximum 2D extent of the leader channel, measured from its origin on the grounded sphere (2) to its most distant point is about 29 $\pm$ 2 cm. It was found from the corresponding IR images (discussed later in this paper), captured with much longer (2.4 ms) exposure time, that the total leader channel length was 42 $\pm$ 1 cm; that is, it did not enter the cloud.

As noted above, current pulse 1 associated with the beginning of the initial corona streamer burst was followed, after a time interval of 2.4 μs, by a multi-peak current waveform. Light emissions of streamers associated with the first two peaks of that current waveform (labeled 2 and 3 in Figure 3b) were likely imaged in the first frame of 4Picos (see Figure 2I). We argue that the UPF occurred before those two subsequent streamer bursts, because the onset of signal from the photomultiplier (viewing the upper part of the cloud, with the region within about 0.5 m of the grounded sphere being outside of its field of view) was ~1.7 μs after the current pulse 1 and 1.9 μs before the current pulse 2. Further, the light intensity of a discharge near the grounded sphere after being scattered by the cloud was below the sensitivity threshold of the photomultiplier. Thus, current measured at the grounded sphere must precede (not follow) the light emission detected by the photomultiplier, which means that the UPF seen in Figure 2I was caused by the streamer burst associated with current pulse 1 (see Figure 3b), as stated above.

Characteristics of current pulses 1 through 4 (see Figure 3b) are summarized in Table 1.

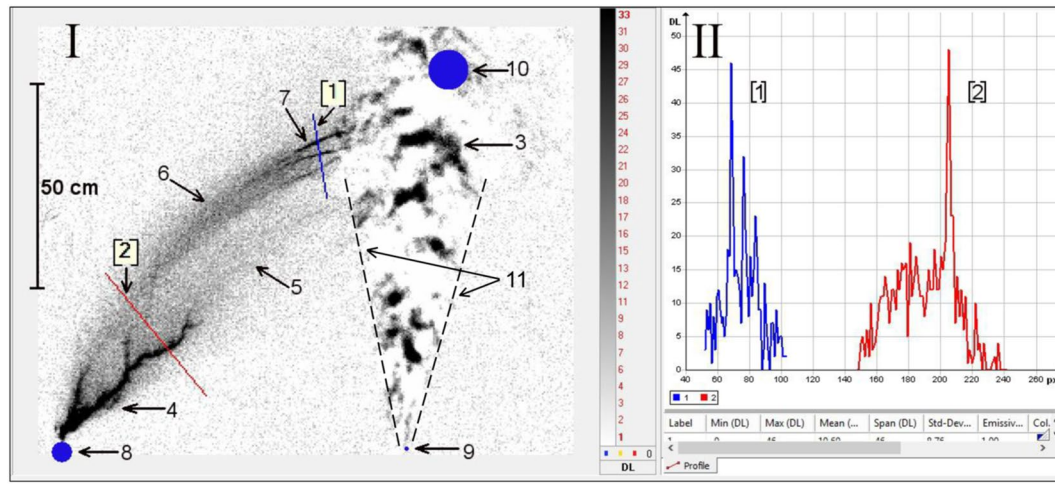

Figure 4. I (Left panel): One frame of event 2015-12-04_03 obtained with an infrared (FLIR) camera (wavelength range: 2.5–5.5 μm, image size 320 × 256 pixels, pixel size 14 × 15 μm, image depth: 14 bit, frame exposure: 2.4 ms, lens focal length: 50 mm, *f*/2, the image is cropped). This infrared image was obtained by subtracting the previous frame from this frame and inverting the differential image. II (Right panel): The IR brightness profiles for hot channel segments within UPF (shown in blue and labeled [1]) and upward positive leader channel (shown in red and labeled [2]), with the corresponding cross-sections being shown in I (left panel). Numbered in I (left panel) are: 3: negatively charged cloud; 4: upward positive leader; 5: streamer zone of the upward positive leader; 6: initial corona streamer burst converted to UPF; 7: hot channel segments within UPF; 8: grounded metal sphere (drawn to scale); 9: center of the grounded plane, where the nozzle (see Figure 1) is located; 10: the region of passage of the microwave beam (drawn to scale); and 11: approximate IR cloud boundary.

Rise time of current pulse 4 is considerably larger than that of the preceding three pulses, which might be indicative of the streamer-to-leader transition (Bazelyan & Raizer, 1998) around the time of pulse 4. With an uncertainty less than 0.2 us, the microwave absorption peak occurred 1.75 μs after current pulse 1 (associated with the streamer burst, within which the UPF was formed (see Figure 2I)), 0.56 μs before the beginning of pulse 2, and 0.71 μs before pulse 3, after which the upward positive leader was initiated from the grounded sphere (see Figure 2II).

The total positive charge transferred to the cloud by the initial corona streamer burst in its entirety and by the following upward leader, estimated by integrating the current waveform from 0 to 50 μs, was 15 μC, which is about a quarter of the typical total (negative) cloud charge.

The upward positive leader is clearly imaged during the 10-μs exposure time of the second 4Picos frame (see Figure 2II). For the first couple of microseconds, when the leader current was 2–3 A, some of the streamers apparently reached the region of passage of the microwave beam (labeled 5 in Figure 2II), as evidenced by the small absorption of microwave radiation seen in Figure 3. Interestingly, the absorption is smaller for current pulse 3, whose peak is appreciably larger (5.8 A). The latter observation may indicate that most of the streamers did not reach the microwave beam.

Figure 4I shows an IR image of the event whose visible-range image is shown in Figure 2. In Figure 4I, the image size is 320 × 256 pixels, and frame exposure time is 2.4 ms. To improve contrast, the presented IR image was obtained by subtracting the previous frame from this one and inverted. With the exposure time of 2.4 ms, almost all discharge processes are imaged (integrated) in the presented single (differential) frame. The relatively hot channel (4) of the branching upward positive leader and its streamer zone (5) reaching the cloud are superimposed on the image of the preceding initial corona streamer burst/UPF (6) with relatively hot channel segments (7). Overall, the IR image is similar to its visible-range counterpart, seen in Figure 2I, but with poorer spatial resolution. Also, the IR image presented in Figure 4I has a lower spatial resolution and brightness compared to the IR images reported previously by Kostinskiy et al. (2015a, 2015b). This is because in the present study images were taken from 2.5 times greater distance, resultant images had four times fewer pixels, and frame exposure time was 3–4 times longer (with the same lens). Nevertheless, all the main features of the discharge are visible in IR image shown in Figure 4I.

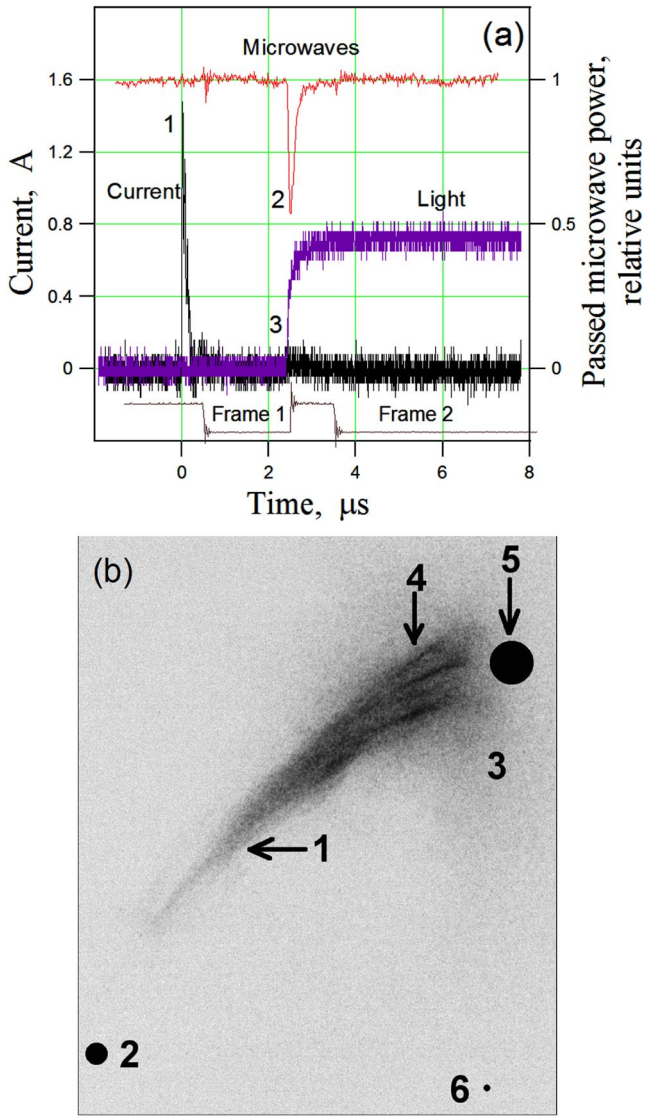

Figure 5. (Event 2015-12-04_14) (a) Current measured at the grounded sphere (shown in black); absorption of microwave radiation that passes through the cloud (shown in red and labeled "Microwaves"); photomultiplier signal (shown in purple and labeled "Light"), and exposure times of 4Picos Frames 1 and 2 (shown in blue), (b) 4Picos Frame 1 (there is no image in Frame 2). The image is cropped. 1: initial corona streamer burst converted to UPF; 2: grounded metal sphere (drawn to scale); 3: cloud of negatively charged water droplets; 4: hot channel segments within UPF; 5: the region of passage of the microwave beam (drawn to scale); and 6: center of the grounded plane, where the nozzle (see Figure 1) is located.

The IR brightness (which represents the energy input to gas) of the channel segments within UPF is similar to that on the channel of upward positive leader, as evidenced by IR brightness profiles shown in Figure 4II for two cross-sections labeled [1] and [2] in Figure 4I. The 2D length of the leader channel without taking into account the branching in the IR image from the starting point on the grounded sphere to the most distant point was about 42 ± 1 cm, which, given the 2.4-ms exposure time, is the total leader channel length for this event. It is longer than 29 ± 2 cm in the visible-range image by 10 cm or so.

We now present an additional event for which the current, light (photomultiplier signal), and microwave absorption were recorded (see Figure 5a) along with a UPF image (see Figure 5b). In contrast with the event presented in Figures 2–4, no leader channel was formed after the initial corona streamer burst. In this case, 40 μs before the initial corona streamer burst and 160 μs after it, microwave absorption and current measured at the grounded sphere do not indicate any discharge activity. The current signature of the initial corona streamer burst is a single submicrosecond-scale pulse labeled 1 in Figure 5a. Figure 5b shows part of the streamer burst (1) that originated on the grounded sphere (2) and propagated to the visible edge of the cloud (3), entered the cloud, and approached almost perpendicularly the region of passage of the microwave beam (5). The streamer heads propagated from the grounded sphere (2) to the microwave beam (5) along an arc distance of about $S_{st} \approx 1.2$ m in about $\tau_{st} \approx 2.4$ μs (measurement accuracy ± 50 ns). The streamer movement inside the cloud is confirmed by the microwave absorption pulse labeled 2 in Figure 5a. The microwave absorption pulse duration (FWHM) was slightly longer than in Figure 3b and was equal to 160 ± 20 ns. The absorption pulse peak was very close to the end of exposure of the 4Picos frame shown in Figure 5b. The average 2D speed of streamers in this case was slightly lower than in Figure 2 and was equal to $v_{st} \approx S_{st}/\tau_{st} \approx 5 \times 10^5$ m/s. In Figure 5b, bright channel segments (labeled 4 in Figure 5b) are seen within the UPF, near the edge of the cloud. The exposure of the first frame of 4Picos (see Figure 5b) started about 600 ns after the onset of the initial corona streamer burst (see current pulse 1 and the leading edge of the exposure pulse corresponding to Frame 1 in Figure 5a); that is, the beginning of the streamer burst was not captured by the 4Picos camera. This is why the lower part of the streamer burst (corresponding to the first 600 ns of its development) appears to be missing in Figure 5b. Note that in Figure 2I, the image of streamer burst corresponds to three current pulses labeled 1, 2, and 3 in Figure 3b.

The current pulse 1 (see Figure 5a) associated with the streamer burst has a peak of about 1.5 A (the rise time of the current pulse is 35 ± 5 ns, the duration of the current pulse at half maximum (FWHM) is 100 ± 10 ns, and the fall time is 190 ± 10 ns). The total charge of the initial corona streamer burst (estimated by integration of measured current) was about 0.3 μC, very small compared to the expected cloud charge of about 60 μC. Relatively hot segments within the UPF in Figure 5b do not look as bright as those in Figure 2I, because they were formed at the end of exposure of the 4Picos frame, as evidenced by the photomultiplier and microwave absorption signals, labeled 3 and 2 in Figure 5a, respectively.

Table 1
Characteristics of Current Pulses 1 Through 4 Labeled in Figure 3b

	Peak current (A)	Rise time (ns)	FWHM (ns)	Fall time (ns)	Interpulse interval relative to pulse 1 (μs)
Pulse 1	1.1	30 ± 5 ns	90 ± 10	147 ± 10	–
Pulse 2	3.14	30 ± 5 ns	–	–	2.42
Pulse 3	5.8	30 ± 5 ns	130 ± 10	180 ± 20	2.58
Pulse 4	3.3	195 ± 10	180 ± 10	210 ± 10	3.08

2. Discussion and Summary

We observed that UPFs, first reported by Kostinskiy et al. (2015b), occurred when the initial (positive) corona streamer burst, initiated from the small grounded sphere, approached and entered the optically visible cloud of negatively charged water droplets. In contrast with ordinary streamer formations (e.g., initial corona streamer burst), UPFs contain presumably hot channel segments that are as bright as leader channels in our IR records and persist for milliseconds (it is in this sense that we refer to them as "hot"; their temperature is actually not known). Importantly, the UPFs occurred prior to the formation (or in the absence) of associated hot leader channel. From this observational fact, we conclude that some kind of streamer-to-leader transition within the initial corona streamer burst is one of the mechanisms behind UPFs. It is presently not clear if the UPFs were caused solely by the enhanced electric field near the charged cloud boundary or other factors also played a role. Within 40 μs prior to the onset of the initial corona streamer burst, no events that could give rise to UPFs were detected. We infer that the streamer burst entering the cloud experienced some kind of instability (e.g., the thermal-ionizational instability (Bychkov et al., 2007; Nighan, 1977; Raizer, 1991, pp. 222–226; Wolf et al., 2020; Zhong et al., 2019)) giving rise to UPFs.

Using current and low-light recordings in conjunction with the microwave sounding of the cloud, we found that hot channel segments within UPFs were formed in very short times of the order of 1 μs or less. These times are consistent with the characteristic time of development of the streamer-to-leader transition in air at atmospheric pressure (Bazelyan et al., 2007; Popov, 2009). Note also that Suzuki (1971) found, from laboratory experiments with discharges in 1- to 4-cm positive point-to-plane gaps, that thermalization (streamer-to-arc transition) occurred in several hundred nanoseconds, provided that the overvoltage exceeded 30%.

In this work, we observed hot channel segments embedded in UPFs, which in part were outside the cloud boundary seen with the visible-range camera. It is likely that the space charge is present not only inside, but also outside of the visible cloud, which can explain those observations. It is worth noting that the hot channel segments within UPF always appear in groups, which probably implies that the occurrence of one such segment creates conditions facilitating the occurrence of additional ones. Occurrence of UPFs may be a necessary component of any lightning initiation scenario (Iudin et al., 2021; Kostinskiy et al., 2020).

It is known that negative leaders in long sparks and lightning developing in virgin air extend in a stepped manner, with the step formation process involving a space leader that originates ahead of the leader tip (inside or near the streamer zone), extends bidirectionally, and eventually makes connection to the primary channel. Since the space leader is self-propagating, it should be hot, and as such it may be similar in some respects to hot segments of UPFs discussed in this paper. The first reasonably complete and clear description of the negative leader stepping process (including the space leader) is due to Gorin et al. (1976, Figure 2a). Space leaders in negative natural and rocket-triggered lightning were observed by Biagi et al. (2010, 2014), Petersen and Beasley (2013), Tran et al. (2014), Gamerota et al. (2014), Qi et al. (2016), and Khounate et al. (2021), among others, and modeled by Syssoev et al. (2020). There is a growing body of evidence that positive leaders in long sparks and lightning can also involve space leaders formed inside or near the streamer zone extending from the leader tip (see Huang, Chen, Fu, Fu, et al., 2022; Huang, Chen, Fu, Xiang, et al., 2022; Huang et al., 2021; Kostinskiy et al., 2018). Space leaders were also observed inside the common streamer zone of the breakthrough phase of the lightning (Biagi et al., 2009; Gamerota et al., 2015) and long spark (Fu et al., 2022) attachment process.

As noted above, it is possible that space leaders have something in common with hot channel segments of UPFs discussed in this paper. Both can be viewed as elevated-temperature plasma formations occurring inside or near the regions filled with cold streamers. There are, however, at least two significant differences: (a) UPFs usually exhibit complex network-like morphology, not seen in space leaders and (b) UPFs can include segments that remain hot for at least some milliseconds (Kostinskiy et al., 2015a, 2015b; Figure 2), while space leaders occur on a much shorter (microsecond) time scale.

It is worth noting that UPFs are different from the so-called "pilot systems" observed by Kochkin et al. (2014, 2015) in the meter-scale gaps subjected to voltage impulses with a risetime of the order of 1 μs. They defined the "pilot system" as a bidirectional structure composed of "positive corona," "negative corona," and "space stem" (one of

the "streamer beads" left behind by preceding negative streamers), as seen in Figure 11 of Kochkin et al. (2015). It follows from this definition that the "pilot system" is a pure streamer formation without any hot segments (which are a distinctive feature of UPFs). Kochkin et al. (2015, p. 8) hypothesized that "in larger gaps of a few meters, the pilot system can even develop into a space leader." The lack of hot channel segments in the "pilot system" makes it different from UPFs presented in this study.

The main findings of the present study can be summarized as follows:

1. UPFs can occur inside the initial corona streamer burst, before the development (or in the absence) of a hot leader channel. This is the only context of UPF occurrence that we observed in this study, but other scenarios are likely to exist.
2. UPFs contain hot channel segments that are formed, possibly via the thermal-ionizational instability, on a time scale of the order of 1 μs or less. These hot channel segments may be similar in some respects to the space leaders involved in the primary-leader step formation process.
3. UPFs occurred in the vicinity of cloud boundary, where the electric field is highest, as this boundary is penetrated by the streamer burst. Further studies are needed to better understand the role of the presence of turbulent, warm cloud in the UPF formation process.

Data Availability Statement

All the data and results for event 2015-12-04_03 can be found at https://doi.org/10.6084/m9.figshare.20097098.v1.

Acknowledgments
This work was an output of a research project carried out as part of the Basic Research Program at the National Research University Higher School of Economics (HSE University). The authors are grateful to the Russian Science Foundation Grant No. 19-17-00218 for supporting this research and to Ekaterina Svechnikova for help in preparing figures. The microwave diagnostics work was supported in part by the Russian Science Foundation Grant No. 19-19-00501-P. Participation of V. A. Rakov was supported in part by the NSF Grant No. AGS-2114471. Ziqin Ding helped with finalizing Figure 4. Ute Ebert and two anonymous reviewers provided useful comments.

References

Bazelyan, E. M., & Raizer, Y. P. (1998). *Spark discharge*. CRC Press.
Bazelyan, E. M., Raizer, Y. P., & Aleksandrov, N. L. (2007). The effect of reduced air density on streamer-to-leader transition and on properties of long positive leader. *Journal of Physics D: Applied Physics*, *40*(14), 4133–4144. https://doi.org/10.1088/0022-3727/40/14/007
Biagi, C. J., Jordan, D. M., Uman, M. A., Hill, J. D., Beasley, W. H., & Howard, J. (2009). High-speed video observations of rocket-and-wire initiated lightning. *Geophysical Research Letters*, *36*(15), L15801. https://doi.org/10.1029/2009GL038525
Biagi, C. J., Uman, M. A., Hill, J. D., & Jordan, D. M. (2014). Negative leader step mechanisms observed in altitude triggered lightning. *Journal of Geophysical Research: Atmospheres*, *119*(13), 8160–8168. https://doi.org/10.1002/2013JD020281
Biagi, C. J., Uman, M. A., Hill, J. D., Jordan, D. M., Rakov, V. A., & Dwyer, J. (2010). Observations of stepping mechanisms in a rocket-and-wire triggered lightning flash. *Journal of Geophysical Research*, *115*(23), 2–7. https://doi.org/10.1029/2010JD014616
Bogatov, N. A., Kostinskiy, A. Y., Syssoev, V. S., Andreev, M. G., Bulatov, M. U., Sukharevsky, D. I., et al. (2020). Experimental investigation of the streamer zone of long-spark positive leader using high-speed photography and microwave probing. *Journal of Geophysical Research: Atmospheres*, *123*(11), e2019JD031826. https://doi.org/10.1029/2019JD031826
Bychkov, V. L., Grachev, L. P., & Isakov, I. I. (2007). Thermal ionization instability of an air discharge plasma in a microwave field. *Technical Physics*, *52*(3), 289–295. https://doi.org/10.1134/S1063784207030012
Francisco, H., Teunissen, J., Bagheri, B., & Ebert, U. (2021). Simulations of positive streamers in air in different electric fields: Steady motion of solitary streamer heads and the stability field. *Plasma Sources Science and Technology*, *30*(11), 115007. https://doi.org/10.1088/1361-6595/ac2f76
Fu, Y., Chen, W., Zhao, Y., Ding, L., Fu, Z., Xiang, N., et al. (2022). Observations of the breakthrough phase of attachment process in laboratory long sparks. *Geophysical Research Letters*, *49*(16), e2022GL099193. https://doi.org/10.1029/2022GL099193
Gamerota, W. R., Idone, V. P., Uman, M. A., Ngin, T., Pilkey, J. T., & Jordan, D. M. (2014). Dart-stepped-leader step formation in triggered lightning. *Geophysical Research Letters*, *41*(6), 2204–2211. https://doi.org/10.1002/2014GL059627
Gamerota, W. R., Uman, M. A., Hill, J. D., & Jordan, D. M. (2015). Observations of corona in triggered dart-stepped leaders. *Geophysical Research Letters*, *42*(6), 1977–1983. https://doi.org/10.1002/2014GL062911
Gorin, B. N., Levitov, V. I., & Shkilev, A. V. (1976). Some principles of leader discharge of air gaps with a strong non-uniform field. *IEEE Conference Publication*, *143*, 274–278.
Huang, S., Chen, W., Fu, Z., Fu, Y., Xiang, N., Qiu, X., et al. (2022). Separate luminous structures leading positive leader steps. *Nature Communications*, *13*(1), 3655. https://doi.org/10.1038/s41467-022-31409-x
Huang, S., Chen, W., Fu, Z., Shi, W., Xiang, N., Fu, Y., et al. (2021). Polarity symmetry of leaders in moist air. *Research Square* (preprint). https://doi.org/10.21203/rs.3.rs-279403/v1
Huang, S., Chen, W., Fu, Z., Xiang, N., Ding, Y., Cheng, D., et al. (2022). On the step type of continuous propagating positive leader in laboratory-scale long spark discharges. *Geophysical Research Letters*, *49*(12), e2022GL097890. https://doi.org/10.1029/2022GL097890
Iudin, D. I., Rakov, V. A., Syssoev, A. A., Bulatov, A. A., & Hayakawa, M. (2021). From decimeter-scale elevated ionic conductivity regions in the cloud to lightning initiation. *Nature Scientific Reports*, *11*(1), 18016. https://doi.org/10.1038/s41598-021-97321-4
Khounate, H., Nag, A., Plaisir, M. N., Imam, A. Y., Biagi, C. J., & Rassoul, H. K. (2021). Insights on space-leader characteristics and evolution in natural negative cloud-to-ground lightning. *Geophysical Research Letters*, *48*(16), 1–9. https://doi.org/10.1029/2021GL093614
Kochkin, P. O., van Deursen, A. P. J., & Ebert, U. (2014). Experimental study of the spatio-temporal development of metre-scale negative discharge in air. *Journal of Physics D: Applied Physics*, *47*(14), 145203. https://doi.org/10.1088/0022-3727/47/14/145203
Kochkin, P. O., van Deursen, A. P. J., & Ebert, U. (2015). Experimental study on hard X-rays emitted from metre-scale negative discharges in air. *Journal of Physics D: Applied Physics*, *48*(2), 025205. https://doi.org/10.1088/0022-3727/48/2/025205

Kossyi, I. A., Kostinsky, A. Y., Matveev, A. A., & Silakov, V. P. (1992). Kinetic scheme of the non-equilibrium discharge in nitrogen–oxygen mixtures. *Plasma Sources Science and Technology*, *1*(3), 207–220. https://doi.org/10.1088/0963-0252/1/3/011

Kostinskiy, A. Y., Marshall, T. C., & Stolzenburg, M. (2020). The mechanism of the origin and development of lightning from initiating event to initial breakdown pulses (v.2). *Journal of Geophysical Research: Atmospheres*, *125*(22), e2020JD033191. https://doi.org/10.1029/2020JD033191

Kostinskiy, A. Y., Syssoev, V. S., Bogatov, N. A., Mareev, E. A., Andreev, M. G., Bulatov, M. U., et al. (2018). Abrupt elongation (stepping) of negative and positive leaders culminating in an intense corona streamer burst: Observations in long sparks and implications for lightning. *Journal of Geophysical Research: Atmospheres*, *123*(10), 5360–5375. https://doi.org/10.1029/2017JD027997

Kostinskiy, A. Y., Syssoev, V. S., Bogatov, N. A., Mareev, E. A., Andreev, M. G., Bulatov, M. U., et al. (2016). Observations of the connection of positive and negative leaders in meter-scale electric discharges generated by clouds of negatively charged water droplets. *Journal of Geophysical Research: Atmospheres*, *121*(16), 9756–9766. https://doi.org/10.1002/2016JD025079

Kostinskiy, A. Y., Syssoev, V. S., Bogatov, N. A., Mareev, E. A., Andreev, M. G., Makalsky, L. M., et al. (2015a). Infrared images of bidirectional leaders produced by the cloud of charged water droplets. *Journal of Geophysical Research: Atmospheres*, *120*(20), 10728–10735. https://doi.org/10.1002/2015JD023827

Kostinskiy, A. Y., Syssoev, V. S., Bogatov, N. A., Mareev, E. A., Andreev, M. G., Makalsky, L. M., et al. (2015b). Observation of a new class of electric discharges within artificial clouds of charged water droplets and its implication for lightning initiation within thunderclouds. *Geophysical Research Letters*, *42*(19), 8165–8171. https://doi.org/10.1002/2015GL065620

Li, X., Guo, B., Sun, A., Ebert, U., & Teunissen, J. (2022). A computational study of steady and stagnating positive streamers in N_2–O_2 mixtures. *Plasma Sources Science and Technology*, *31*(6), 065011. https://doi.org/10.1088/1361-6595/ac7747

Nighan, W. L. (1977). Causes of thermal instability in externally sustained molecular discharges. *Physical Review A*, *15*(4), 1701–1720. https://doi.org/10.1103/PhysRevA.15.1701

Nijdam, S., Teunissen, J., & Ebert, U. (2020). The physics of streamer discharge phenomena. *Plasma Sources Science and Technology*, *29*(10), 103001. https://doi.org/10.1088/1361-6595/abaa05

Petersen, D. A., & Beasley, W. H. (2013). High-speed video observations of a natural negative stepped leader and subsequent dart-stepped leader. *Journal of Geophysical Research: Atmospheres*, *118*(21), 1–10. https://doi.org/10.1002/2013JD019910

Popov, N. A. (2009). Study of the formation and propagation of a leader channel in air. *Plasma Physics Reports*, *35*(9), 785–793. https://doi.org/10.1134/S1063780X09090074

Qi, Q., Lu, V., Ma, Y., Chen, L., Zhang, Y., & Rakov, V. (2016). High-speed video observations of the fine structure of a natural negative stepped leader at close distance. *Atmospheric Research*, *178–179*, 260–267. https://doi.org/10.1016/j.atmosres.2016.03.027

Raizer, Y. (1991). *Gas discharge physics* (p. 449). Springer-Verlag.

Suzuki, T. (1971). Transition from the primary streamer to the arc in positive point-to-plane corona. *Journal of Applied Physics*, *42*(10), 3766–3777. https://doi.org/10.1063/1.1659684

Syssoev, A. A., Iudin, D. I., Bulatov, A. A., & Rakov, V. A. (2020). Numerical simulation of stepping and branching processes in negative lightning leaders. *Journal of Geophysical Research: Atmospheres*, *125*(7), e2019JD031360. https://doi.org/10.1029/2019JD031360

Tran, M. D., Rakov, V. A., & Mallick, S. (2014). A negative cloud-to-ground flash showing a number of new and rarely observed features. *Geophysical Research Letters*, *41*(18), 6523–6529. https://doi.org/10.1002/2014GL061169

Wolf, A. J., Righart, T. W. H., Peeters, F. J. J., Bongers, W. A., & van de Sanden, M. C. M. (2020). Implications of thermo-chemical instability on the contracted modes in CO_2 microwave plasmas. *Plasma Sources Science and Technology*, *29*(2), 025005. https://doi.org/10.1088/1361-6595/ab5eca

Zhong, H., Shneider, M. N., Mokrov, M. S., & Ju, Y. (2019). Thermal-chemical instability of weakly ionized plasma in a reactive flow. *Journal of Physics D: Applied Physics*, *52*(48), 484001. https://doi.org/10.1088/1361-6463/ab3d69